Supplementary material for N. Mayot, C. Le Quéré, C. Rödenbeck, R. Bernardello, L. Bopp, L. M. Djeutchouang, M. Gehlen, L. Gregor, N. Gruber, J. Hauck, Y. Iida, T. Ilyina, R. F. Keeling, P. Landschützer, A. C. Manning, L. Patara, L. Resplandy, J. Schwinger, R. Séférian, A. J. Watson, R. M. Wright and J. Zeng, 2023, Climate-driven variability of the Southern Ocean CO_2 sink, *Phil. Trans. R. Soc. A.* doi: 10.1098/rsta.2022.0055

Ocean modelling protocol from RECCAP2-ocean

Here, we are summarizing the ocean modelling protocol provided by RECCAP2. The entire protocol can be downloaded at this website: https://reccap2-ocean.github.io/protocols/

All modelling groups conducted the simulations A and C. These two simulations vary in terms of their atmospheric forcing (time varying versus climatological, Table S1).

The simulation A had to reproduce the interannual variability and trend in the ocean carbon uptake in response to changes in both atmospheric CO_2 and climate. Thus, models should be forced by observed climate (e.g. from reanalysis products) and observed atmospheric CO_2 throughout the entire time period. No specified products were recommended, but RECCAP2 required continuity in forcing, i.e. only one forcing data should be used for the full time-series of the analysis period, i.e., 1980 through 2018. Similarly, all modelling groups could use their own atmospheric CO_2 time-series or the one provided by RECCAP2.

The initialization and spinup strategy that has to be pursued was: an initialization from preindustrial conditions, followed by a long spinup. Thus, the ocean was initialized from (reconstructed) preindustrial conditions and then spun up for several decades to centuries in order to ensure minimal drift in the surface fluxes. The models were then brought forward in time to the analysis period using either constant atmospheric forcing until the reanalysis period begins or by cycling through the atmospheric forcing time-series.

Table S1. Summary of simulations A and C.

	Simulation A	**Simulation C**
Atmospheric CO_2	Increasing	Increasing
Atmospheric forcing (wind, fluxes of heat and freshwater)	Variable, reanalysis	Climatological
Considered components(*)	$Flux_{ant}^{ss} + Flux_{ant}^{ns} + Flux_{nat}^{ss} + Flux_{nat}^{ns}$	$Flux_{ant}^{ss} + Flux_{nat}^{ss}$

*Total Flux = $Flux_{ant}^{ss} + Flux_{ant}^{ns} + Flux_{nat}^{ss} + Flux_{nat}^{ns}$, where $Flux_{ant}$ and $Flux_{nat}$ are the air-sea fluxes of anthropogenic and natural CO_2, respectively. $Flux_{ant}^{ss}$ is equivalent to the effect of rising CO_2 alone on the ocean carbon sink, $Flux_{nat}^{ns} + Flux_{ant}^{ns}$ is the effect of climate change and variability on the ocean carbon sink, and $Flux_{nat}^{ss}$ are the fluxes of natural CO_2 in a constant or preindustrial climate.

Supplementary material for N. Mayot, C. Le Quéré, C. Rödenbeck, R. Bernardello, L. Bopp, L. M. Djeutchouang, M. Gehlen, L. Gregor, N. Gruber, J. Hauck, Y. Iida, T. Ilyina, R. F. Keeling, P. Landschützer, A. C. Manning, L. Patara, L. Resplandy, J. Schwinger, R. Séférian, A. J. Watson, R. M. Wright and J. Zeng, 2023, Climate-driven variability of the Southern Ocean CO_2 sink, *Phil. Trans. R. Soc. A.* doi: 10.1098/rsta.2022.0055

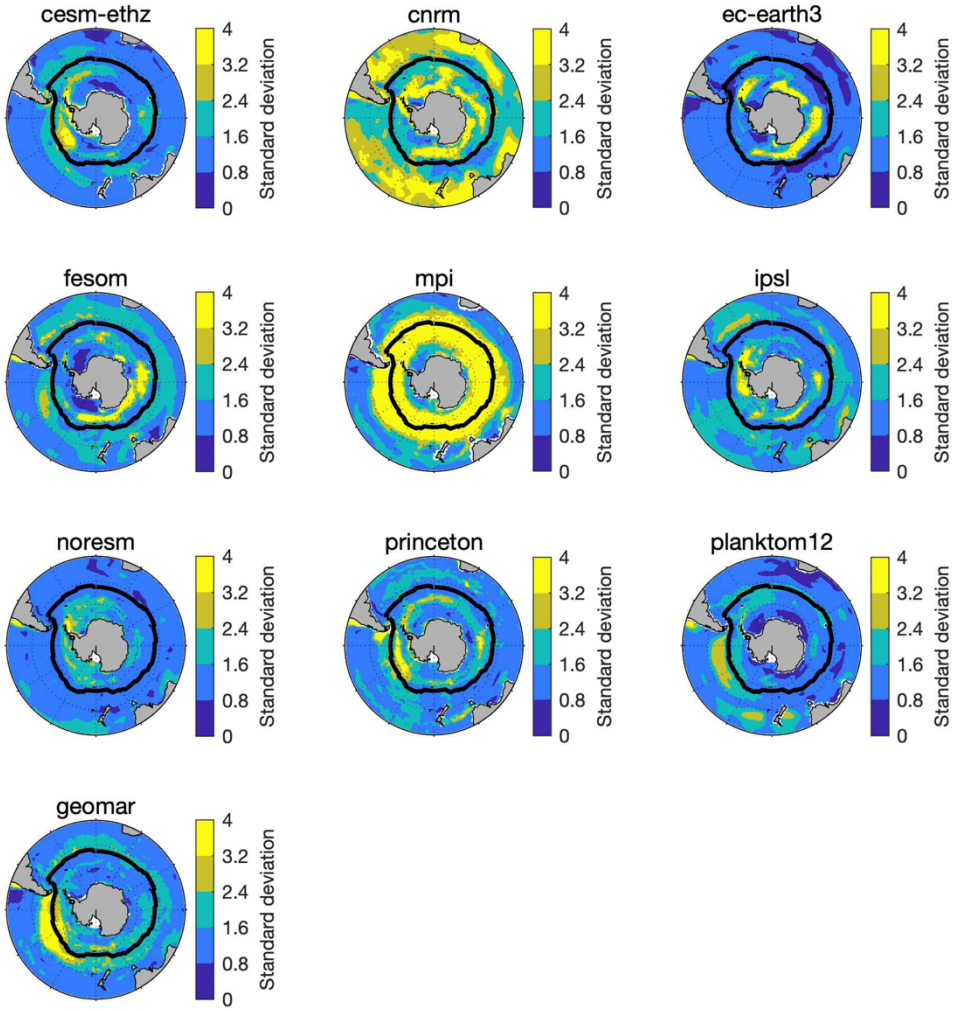

Supplementary Figure 1: Spatial patterns associated with the interannual variability of CO_2 air-sea fluxes for all GOBMs. For each GOBM and at each grid cell, the signal decomposition method was applied, and the standard deviation associated with the interannual component was mapped. The black line represents the averaged location of the subantarctic front.

Supplementary material for N. Mayot, C. Le Quéré, C. Rödenbeck, R. Bernardello, L. Bopp, L. M. Djeutchouang, M. Gehlen, L. Gregor, N. Gruber, J. Hauck, Y. Iida, T. Ilyina, R. F. Keeling, P. Landschützer, A. C. Manning, L. Patara, L. Resplandy, J. Schwinger, R. Séférian, A. J. Watson, R. M. Wright and J. Zeng, 2023, Climate-driven variability of the Southern Ocean CO_2 sink, *Phil. Trans. R. Soc. A.* doi: 10.1098/rsta.2022.0055

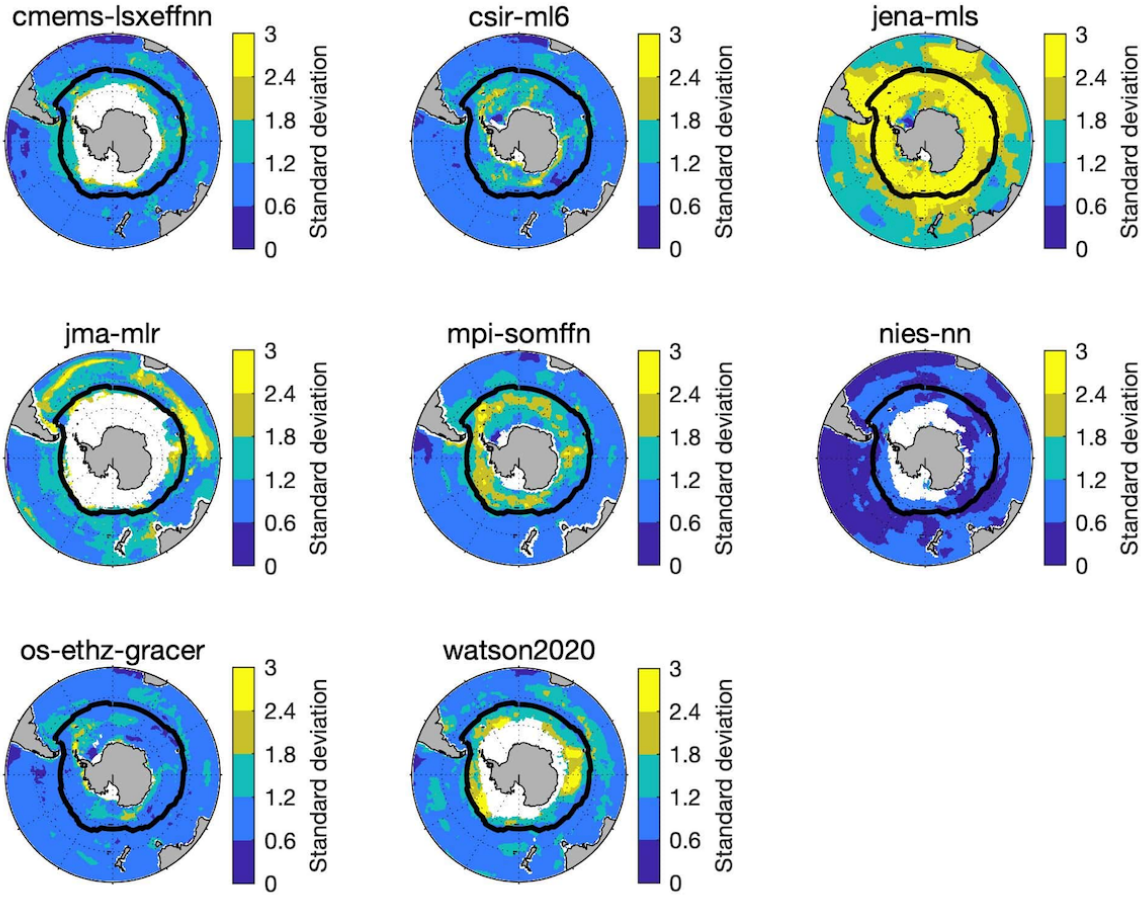

Supplementary Figure 2: Spatial patterns associated with the interannual variability of CO_2 air-sea fluxes for all pCO_2 products. For each pCO_2 products and at each grid cell, the signal decomposition method was applied, and the standard deviation associated with the interannual component was mapped. The black line represents the averaged location of the subantarctic front.

Supplementary material for N. Mayot, C. Le Quéré, C. Rödenbeck, R. Bernardello, L. Bopp, L. M. Djeutchouang, M. Gehlen, L. Gregor, N. Gruber, J. Hauck, Y. Iida, T. Ilyina, R. F. Keeling, P. Landschützer, A. C. Manning, L. Patara, L. Resplandy, J. Schwinger, R. Séférian, A. J. Watson, R. M. Wright and J. Zeng, 2023, Climate-driven variability of the Southern Ocean CO_2 sink, *Phil. Trans. R. Soc. A.* doi: 10.1098/rsta.2022.0055

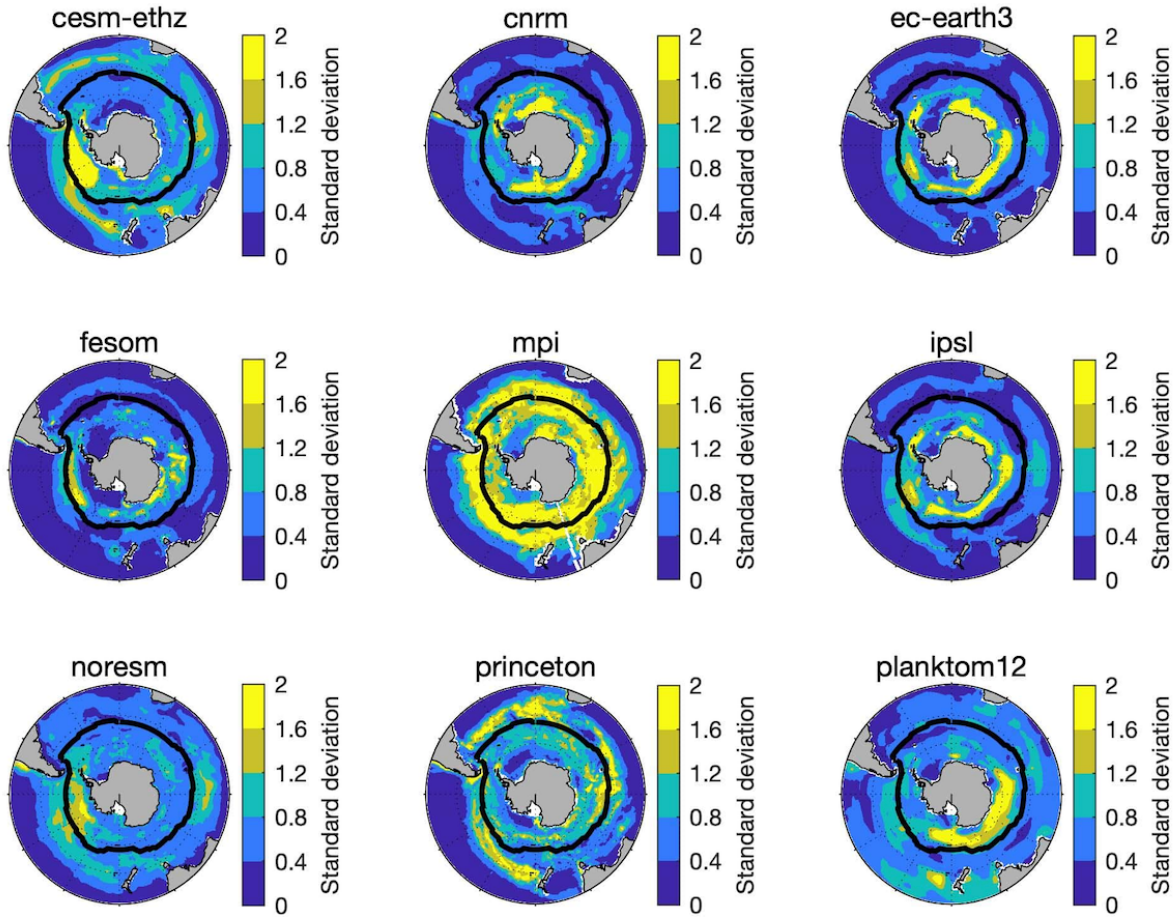

Supplementary Figure 3: Spatial patterns associated with the interannual variability of O_2 air-sea fluxes for all GOBMs. For each GOBMs and at each grid cell, the signal decomposition method was applied, and the standard deviation associated with the interannual component was mapped. The black line represents the averaged location of the subantarctic front.

Supplementary material for N. Mayot, C. Le Quéré, C. Rödenbeck, R. Bernardello, L. Bopp, L. M. Djeutchouang, M. Gehlen, L. Gregor, N. Gruber, J. Hauck, Y. Iida, T. Ilyina, R. F. Keeling, P. Landschützer, A. C. Manning, L. Patara, L. Resplandy, J. Schwinger, R. Séférian, A. J. Watson, R. M. Wright and J. Zeng, 2023, Climate-driven variability of the Southern Ocean CO_2 sink, *Phil. Trans. R. Soc. A.* doi: 10.1098/rsta.2022.0055

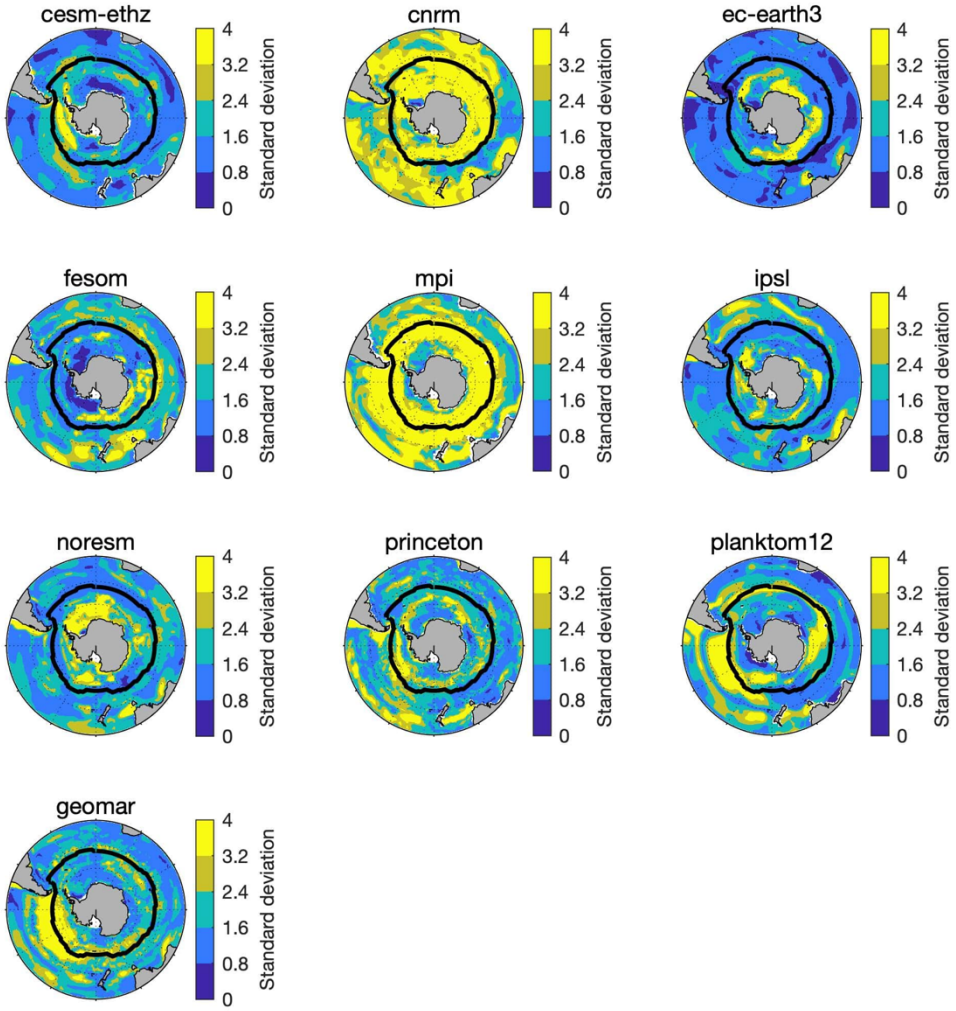

Supplementary Figure 4: Same as figure S1, but for the decadal variability of CO_2 air-sea fluxes.

Supplementary material for N. Mayot, C. Le Quéré, C. Rödenbeck, R. Bernardello, L. Bopp, L. M. Djeutchouang, M. Gehlen, L. Gregor, N. Gruber, J. Hauck, Y. Iida, T. Ilyina, R. F. Keeling, P. Landschützer, A. C. Manning, L. Patara, L. Resplandy, J. Schwinger, R. Séférian, A. J. Watson, R. M. Wright and J. Zeng, 2023, Climate-driven variability of the Southern Ocean CO_2 sink, *Phil. Trans. R. Soc. A.* doi: 10.1098/rsta.2022.0055

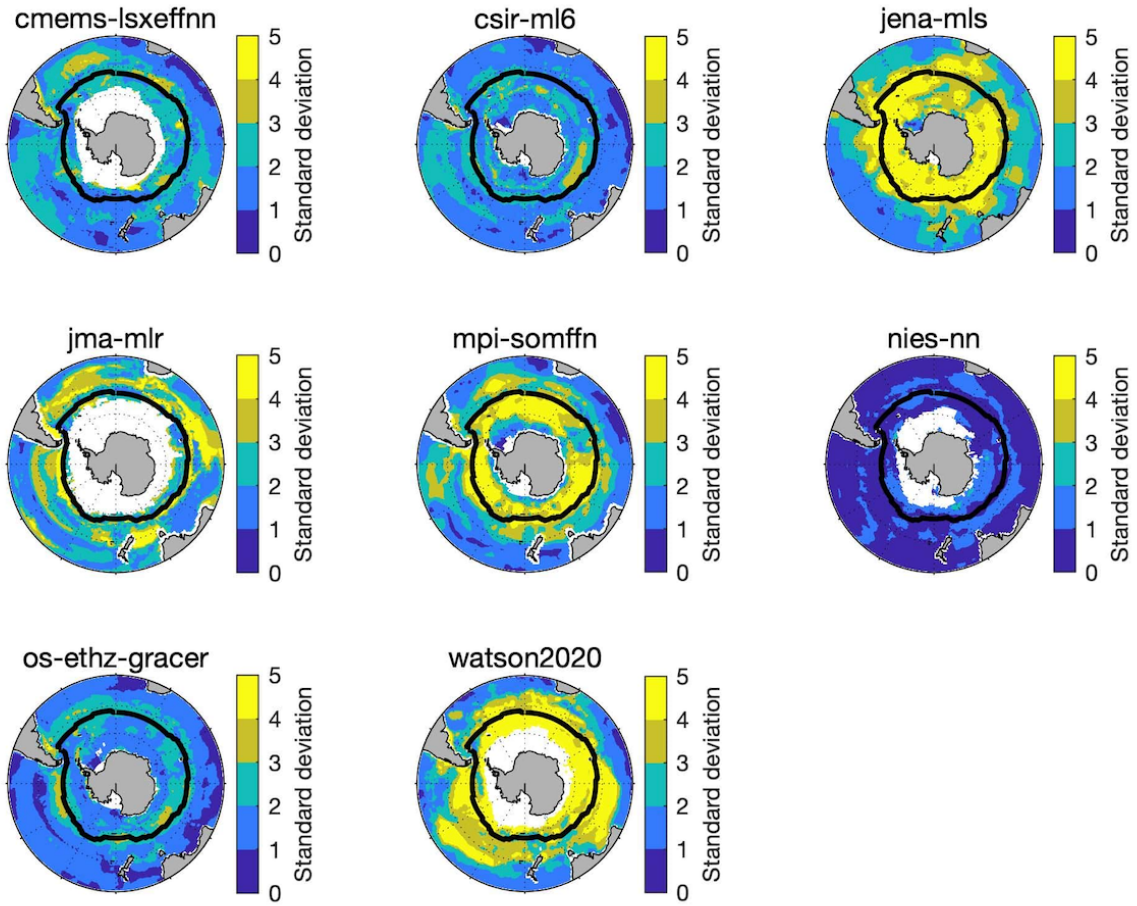

Supplementary Figure 5: Same as figure S2, but for the decadal variability of CO_2 air-sea fluxes.

Supplementary material for N. Mayot, C. Le Quéré, C. Rödenbeck, R. Bernardello, L. Bopp, L. M. Djeutchouang, M. Gehlen, L. Gregor, N. Gruber, J. Hauck, Y. Iida, T. Ilyina, R. F. Keeling, P. Landschützer, A. C. Manning, L. Patara, L. Resplandy, J. Schwinger, R. Séférian, A. J. Watson, R. M. Wright and J. Zeng, 2023, Climate-driven variability of the Southern Ocean CO_2 sink, *Phil. Trans. R. Soc. A.* doi: 10.1098/rsta.2022.0055

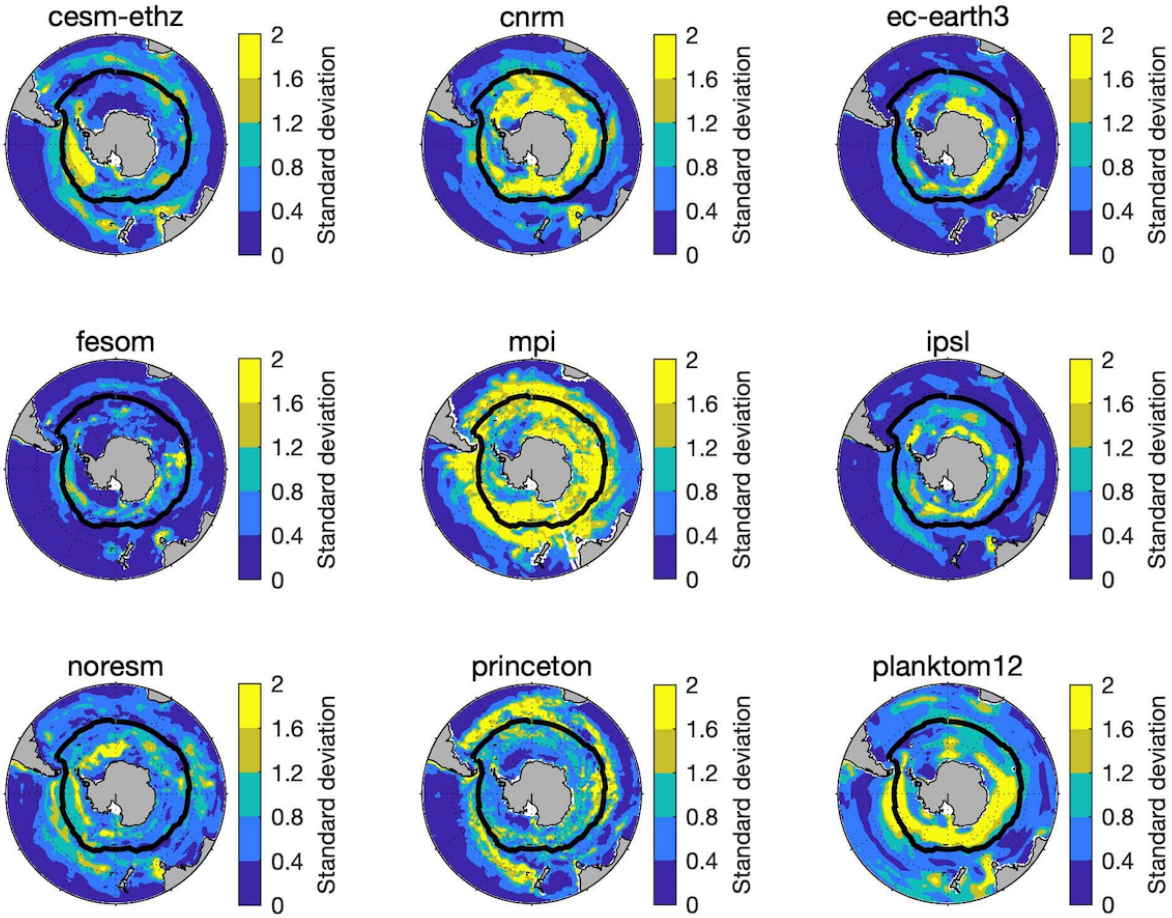

Supplementary Figure 6: Same as figure S3, but for the decadal variability of O_2 air-sea fluxes.

Supplementary material for N. Mayot, C. Le Quéré, C. Rödenbeck, R. Bernardello, L. Bopp, L. M. Djeutchouang, M. Gehlen, L. Gregor, N. Gruber, J. Hauck, Y. Iida, T. Ilyina, R. F. Keeling, P. Landschützer, A. C. Manning, L. Patara, L. Resplandy, J. Schwinger, R. Séférian, A. J. Watson, R. M. Wright and J. Zeng, 2023, Climate-driven variability of the Southern Ocean CO_2 sink, *Phil. Trans. R. Soc. A.* doi: 10.1098/rsta.2022.0055

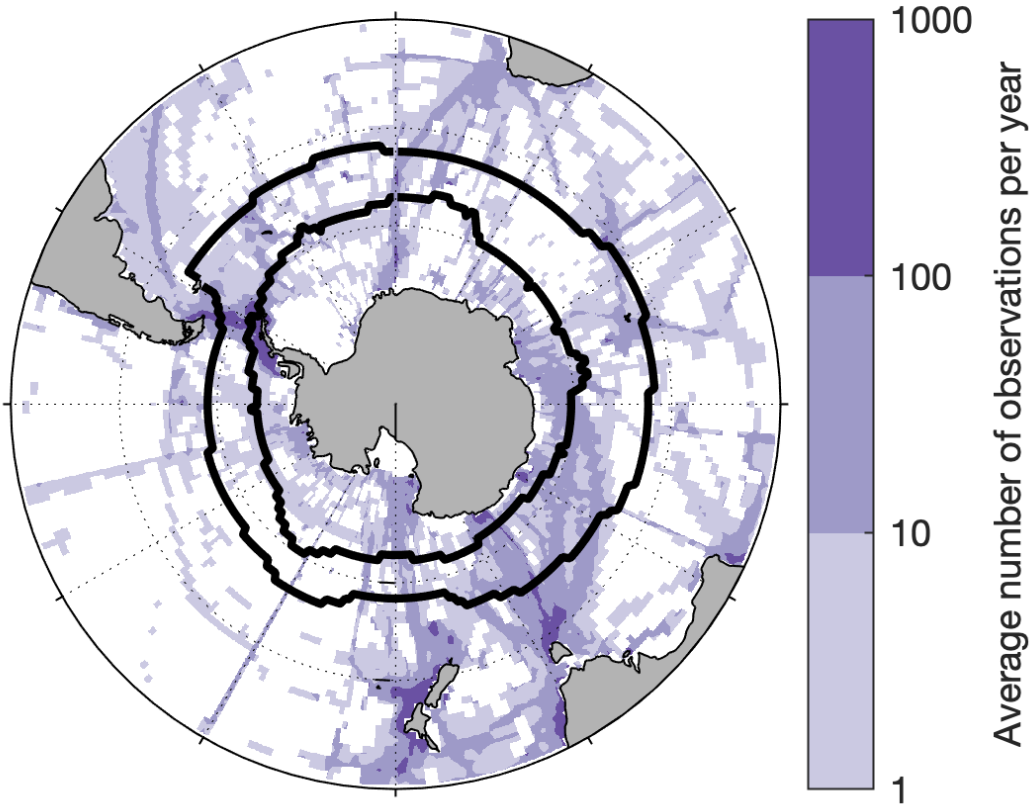

Supplementary Figure 7: Spatial distribution of SOCAT observation density between 1985 and 2018. The black lines represent the averaged location of the Subantarctic Front and of the September extent of sea ice.